A MULTISCALE AND MULTIDISCIPLINARY INVESTIGATION OF ECOSYSTEM–ATMOSPHERE CO_2 EXCHANGE OVER THE ROCKY MOUNTAINS OF COLORADO

BY JIELUN SUN, STEVEN P. ONCLEY, SEAN P. BURNS, BRITTON B. STEPHENS, DONALD H. LENSCHOW, TERESA CAMPOS, RUSSELL K. MONSON, DAVID S. SCHIMEL, WILLIAM J. SACKS, STEPHAN F. J. DE WEKKER, CHUN-TA LAI, BRIAN LAMB, DENNIS OJIMA, PATRICK Z. ELLSWORTH, LEONEL S. L. STERNBERG, SHARON ZHONG, CRAIG CLEMENTS, DAVID J. P. MOORE, DEAN E. ANDERSON, ANDREW S. WATT, JIA HU, MARK TSCHUDI, STEVEN AULENBACH, EUGENE ALLWINE, AND TERESA COONS

A field study combined with modeling investigation demonstrates that the organization of CO_2 transport by mountain terrain strongly affects the regional CO_2 budget.

By conducting model–data assimilation analysis of the long-term eddy covariance dataset from the Niwot Ridge AmeriFlux site operated by the University of Colorado, Schimel et al. (2002), Sacks et al. (2006, 2007), Monson et al. (2005, 2006a,b), and Moore et al. (2008) showed that 1) an aggrading Rocky Mountain subalpine forest is a net annual CO_2 sink, 2) most of the annual CO_2 uptake occurs in spring when melting snow provides moisture for photosynthesis and low soil temperature inhibits respiration, and 3) the interannual variability of forest CO_2 uptake is largely driven by spring conditions. Studies at the same forest site showed, however, that accurate estimates of ecosystem CO_2 exchange are difficult to obtain because the terrain forces us to consider terms that are otherwise ignored in systems with seemingly simpler terrain (Yi et al. 2005; Sun et al. 2007; Yi et al. 2008). Using a biogeochemistry model driven by historical climate data, Schimel et al. (2002) found that ~50% of the western U.S. carbon sink occurs over hilly or mountainous topography with elevations above 750 m. Because a significant fraction of forests worldwide occur in hilly and mountainous terrain, and because this terrain imposes unique challenges to the quantification of local and regional CO_2 budgets, there is a need to develop new types of observations and modeling approaches.

Traditionally, foresters and ecologists have relied on biometric measurements of forest productivity. More recently, chamber-based methods have allowed for some potential to scale these measurements up to the ecosystem or landscape [as an example, we refer the reader to the numerous articles in the special issue of Boreal Ecosystem–Atmosphere Study (BOREAS) studies in the December 1996 publication of the *Journal of Geophysical Research* (vol. 102)]. However, these approaches are limited to a small sampling area and are biased toward measurement-accessible locations (Clark et al. 2001; Ryan and Law 2005). Monitoring CO_2 transport using micrometeorological methods pro-

vides effective investigations of ecosystem–atmosphere exchange over a relatively large area (Baldocchi 2003). Gough et al. (2008) showed that convergence of the two methods can build confidence in estimates of the carbon net ecosystem exchange (NEE; following Chapin et al. 2006). However, most past micrometeorological experiments have been conducted with the assumption of horizontal homogeneity over "idealized" land surfaces even if those assumptions are likely to have been violated by the complexity of the real terrain. Because of complicated carbon sources/sinks associated with plant distributions over heterogeneous surfaces, regardless of whether the surface is flat or not, the traditional one-dimensional micrometeorological monitoring tower often cannot capture NEE. Atmospheric dynamics can lead to complicated flows generated by inhomogeneous landscapes, topography, or synoptic weather systems. As a result, CO_2 transport occurs in all directions, which severely challenges observational methodology.

To investigate CO_2 exchange between the atmosphere and ecosystems over complex terrain (i.e., heterogeneous landscapes on varying topography), horizontal and vertical CO_2 transport by mean circulations and turbulent fluxes need to be considered. While traditional micrometeorological techniques have been developed for measuring turbulent fluxes, mean circulations can often pose the most difficulty in studying ecosystems in complex terrain. Mean flows with spatial variations of CO_2 concentration in the mountains often produce advective CO_2 fluxes. The role of CO_2 advection in estimating ecosystem–atmosphere carbon exchange has previously been investigated by field experiments (e.g., Aubinet et al. 2003; Staebler and Fitzjarrald 2004; Feigenwinter et al. 2004; Dolman et al. 2006; Ahmadov et al. 2007; Pypker et al. 2007a,b; Lauvaux et al. 2008). In September 2002, we conducted a pilot experiment [The Niwot Ridge experiment (NIWOT02)] at the Niwot Ridge AmeriFlux site to explore the methodology of studying the CO_2 budget including the mean advective transport of CO_2 over complex terrain (Sun et al. 2007). We found that the nighttime-respired CO_2 was mixed with cold air adjacent to the ground and transported to low elevations as we expected. In addition, our observations suggested that the cold CO_2-rich air follows the local slope, channeling the CO_2 to the lowest points on the landscape. In the case of the Niwot Ridge site, this was observed as nighttime accumulation of CO_2 in the 2-m-wide Como Creek stream channel. Because of the density difference between water and cold air, the cold air does not follow the creek channel perfectly and often "spills" over the bank. We use the word "carbonshed" to describe the flow of CO_2-laden air similar to the concept of a watershed, although the word "airshed" has sometimes been used to describe air movement.

Based on our NIWOT02 investigation and the understanding we developed of the dynamics of local mountain flows, we expanded our focus beyond that of the local carbonshed and considered the influence of regional circulation on CO_2 transport. In general, we wanted to connect processes that we had observed to be important at the scale of a single carbonshed to those that might operate at the scale of multiple carbonsheds dispersed across an entire mountainous region. Our specific goals were 1) to understand the role of morning mountain circulations in the disappearance of localized CO_2 pools that had accumulated during the night in mountain valleys and depressions; 2) to investigate how the topographic redistribution of energy, snow, and liquid water affects the spatial variation of surface–atmosphere CO_2 exchange in mountains; 3) to examine controlling parameters in hierarchical scaling models used to extrapolate local CO_2 transport to entire mountain ranges; 4) to comprehend ecological processes that explain the observed CO_2 concentrations and fluxes; 5) to estimate the direction and magnitude of CO_2 fluxes across an entire mountainous region; and 6) to model the

AFFILIATIONS: Sun, Oncley, Burns,* Stephens, Lenschow, Campos, and Watt—National Center for Atmospheric Research,+ Boulder, Colorado; Monson, Moore, Hu, and Tschudi—University of Colorado, Boulder, Colorado; Schimel and Aulenbach—National Ecological Observatory Network, Boulder, Colorado; Sacks—University of Wisconsin—Madison, Madison, Wisconsin; De Wekker—University of Virginia, Charlottesville, Virginia; Lai—San Diego State University, San Diego, California; Lamb, Allwine, and Coons—Washington State University, Pullman, Washington; Ojima—Colorado State University, Fort Collins, Colorado; Ellsworth and Sternberg—University of Miami, Miami, Florida; Zhong—Michigan State University, East Lansing, Michigan; Clements—San José State University, San José, California; Anderson—U.S. Geological Survey, Denver, Colorado
***ADDITIONAL AFFILIATION:** University of Colorado, Boulder, Colorado
+The National Center for Atmospheric Research is sponsored by the National Science Foundation.
CORRESPONDING AUTHOR: Jielun Sun, National Center for Atmospheric Research, P.O. Box 3000, Boulder, CO 80305
E-mail: jsun@ucar.edu

The abstract for this article can be found in this issue, following the table of contents.
DOI:10.1175/2009BAMS2733.1

In final form 17 September 2009

ecosystem carbon uptake over Colorado, especially by forests over mountains.

FIELD EXPERIMENTS. The field campaign consisted of a ground deployment, the Carbon in the Mountains Experiment (CME04), and an aircraft deployment of the National Center for Atmospheric Research (NCAR) C-130, the Airborne Carbon in the Mountains Experiment (ACME04) over the period of spring to fall of 2004 to cover the seasonal variation of ecosystem–atmosphere carbon exchange. The ground campaign was designed to better characterize local CO_2 flows, especially those that occur at night, in a single carbonshed nested within a broader region across which the airborne campaign would operate. The airborne campaign was designed to investigate various strategies for measuring regional CO_2 exchange, to elucidate those regional airflow patterns that participate in redistributing the CO_2 pool that accumulated overnight in local carbonsheds, and to estimate the importance of that redistribution to the regional CO_2 budget. The overall extent of the airborne campaign was 350 km × 350 km in the Rocky Mountain region of Colorado (Fig. 1).

Carbon in the Mountains Experiment. The CME04 site is located in the forest at the Niwot Ridge AmeriFlux site, which is part of the Niwot Ridge Long-Term Ecological Reserve (LTER) about 20 km west of Boulder, Colorado (Monson et al. 2002; Turnipseed et al. 2003). The AmeriFlux site consists of a 27-m tower operated by the University of Colorado (CU) and a 33-m tower and two 10-m towers within about 150 m of the CU tower operated by the U.S. Geological Survey (USGS). These towers have been in operation since 1999. Constrained by snow cover in the early spring, the CME04 field campaign lasted from 10 June (not all instruments started operating on 10 June) to 5 October 2004; that is, the ground campaign commenced after the spring season.

In CME04, we had three principal aims: 1) to understand how CO_2 is transported through the forests, with particular attention to the role of the Como Creek channel, which follows the ~5° sloped terrain; 2) to establish the extent of the locally high CO_2 within the vicinity of the creek using a sulfur hexafluoride (SF_6) release experiment; and 3) to evaluate the potential to use stable CO_2 isotopes to assess elevation dynamics in the nighttime redistribution of respired CO_2. In this subsection, we describe our experimental design for the first two components. The ground-based and airborne isotope analyses are discussed in the section "Ground and airborne isotope observations."

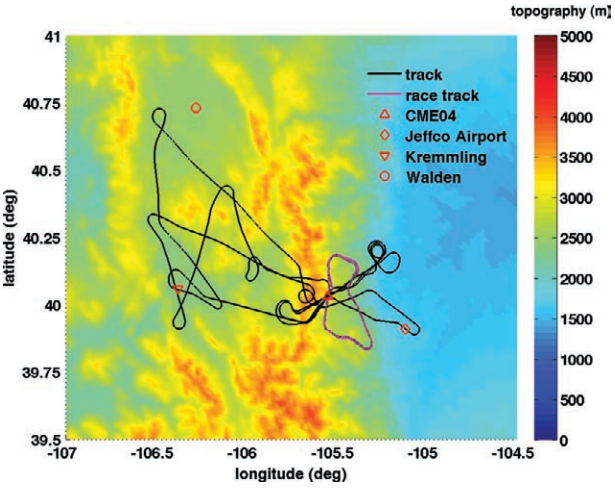

Fig. 1. The track of flight 12 during ACME04.

During NIWOT02, we had found that at night, CO_2 concentration increased along paths that ran toward the ~2-m-wide Como Creek located approximately 300 m from the CU tower (Sun et al. 2007). We expanded the NIWOT02 domain in the design of CME04 to explicitly include a ~300-m section of Como Creek in our observation domain with its upstream, downstream, and cross-creek environment monitored (Fig. 2). To monitor the upstream environment, a 17-m tower was positioned in a 100 m × 100 m open patch covered by ~0.5-m-tall willows surrounded by ~8-m-tall spruce and fir trees ("willow"). To monitor downstream of the creek section, a 30-m tower was erected within a mixed patch dominated by ~10-m-tall aspen trees and ~2-m-tall shrubs ("aspen"). To monitor the spatial variation of the CO_2 transport across Como Creek, CO_2 concentration was measured every 20 m at various heights between a 30-m tower north of Como Creek within a patch of predominantly ~11-m-tall coniferous pine forest ("pine") and the existing CU and USGS towers. Both 30-m towers were ~3 times the canopy height, which enabled us to observe turbulent fluxes above the canopy. The tower locations were selected mainly for monitoring the CO_2 transport along Como Creek over an area of ~1 km^2 and accessibility. In addition, the landscape variation at the three towers offered us opportunities to examine effects of the surface variation on CO_2 transport. The towers were orientated in a diamond shape, which allowed us to fully characterize 2D horizontal transport of CO_2 within the domain. Each tower was equipped to measure turbulent momentum and sensible heat fluxes (at five levels), latent heat fluxes (at two levels), and vertical variations of wind, temperature, water vapor, and CO_2 concentration within and above the canopy layer

Table 1. CME04 instrument deployment.					
Aspen		Pine		Willow	
Z (m)	Variables	Z (m)	Variables	Z (m)*	Variables
30.5	C, T/RH, V_C, T_s, C', Q, R_{net}, PAR	29.7	C, T/RH, V_C, Q, T_s, R_{net}, PAR		
17.6	C, T/RH, V_A	16.8	C, V_{UW}	17	C, T/RH, V_C, T_s, C', Q, R_{net}, PAR
10.3	C, T/RH, V_A, T_s	9.5	C, T/RH, V_{UW}, T_s,	10	C, T/RH, V_A
6.4	C, T/RH, V_G	5.9	C, T/RH, V_{UW}	6	C, T/RH, V_A
		4.0	C		
2.3	C, T/RH, V_C, T_s, C', Q	2.2	C, T/RH, V_C, T_s, C', Q, P_2	2	C, T/RH, V_C, C', Q, P_2
1.2	C, T/RH, V_{UW}, P_2	1.4	C, T/RH, V_{UW}	1	C, T/RH, V_A
				0.5	C

*T/RH are 0.5 m below the height shown except at 1 m.

Z = measurement height (above ground level; AGL).

C = CO_2 concentration measured with two AIRCOA systems—one at aspen and one at willow—and with TGaMS at pine.

C' = fast response CO_2 concentration sampled at 20 Hz and measured with a LI-7000 at aspen, with a LI-6251 at willow, and with a LI-7500 at pine. The vertical CO_2 flux was calculated every 5 min, alternating between two levels at both willow and aspen sites.

T_s = surface radiation temperature measured with Everest4000.4GL sensors.

T/RH = aspirated air temperature and humidity with Vaisala 50Y Humitters.

PAR = photosynthetically active radiation with LI-190.

Q = fast humidity sensor with Campbell model KH20 Krypton hygrometer.

V_C = 3D wind with Campbell CSAT 3-D sonic anemometer sampled at 30 Hz.

V_A = 3D wind with Applied Technologies, Inc., sonic anemometer sampled at 10 Hz.

V_G = 3D wind with Gill model R2 sonic anemometers sampled at 21 Hz.

V_{UW} = 3D wind with NCAR sonic anemometer sampled at 10 Hz.

R_{net} = net radiation with Radiation and Energy Balance System, Inc. model Q*7.

P_2 = pressure measured with Vaisala model PTB220B.

(Table 1). Considering that wind within the canopy can be weak, 3D sonic anemometers were used for the wind profile measurement. Because of our limited number of CO_2/H_2O analyzers, the Hi-Lo method, which was designed by NCAR to switch sampling air at two heights with one CO_2/H_2O analyzer every 5 min, was used to measure CO_2 fluctuations at 10 Hz for calculation of CO_2 and water vapor fluxes. The Hi-Lo method was used at 2 and 17 m with a LI-6251 analyzer at the willow site and at 2 and 30 m with a LI-7000 analyzer at the aspen site to measure the CO_2 and water vapor fluxes within and above the canopy layer. The 5-min Reynolds-averaged fluxes of CO_2 and H_2O were calculated with the box-mean method. The fluxes across any sampling window of 5-min multiples can be calculated based on the time series of the 5-min fluxes, which is described at the Earth Observing Laboratory (EOL) Web site (www.eol.ucar.edu/cme04). An open path LI-7500 CO_2/H_2O analyzer was deployed at the pine tower for measurements of CO_2/H_2O fluxes at 2 m to monitor the CO_2/H_2O fluxes within the canopy. The CO_2/H_2O fluxes at 30 m on the pine tower were assumed to be above the influence of the canopy and similar to those at the highest observation level on the CU/USGS and the aspen towers. Net radiation was measured at the top of all three NCAR towers. A barometric pressure sensor was also installed on each tower. Surface radiation temperatures of the forest floor and the canopy top were measured at the pine and aspen towers. During CME04, a wireless sensor network was successfully tested with NCAR-built soil temperature sensors to measure the spatial variation of the soil temperature associated with different soil types and with sunny and shaded areas. The soil temperature was measured at four stations around each tower. Each station had six probes for measuring soil temperature profiles at 5-, 10-, and 15-cm depths, and soil temperatures at 5 cm at three other locations within an area of about 2 m^2. The soil temperature data were wirelessly transmitted to a central computer. All of the air temperature and humidity sensors during CME04 were

sheltered from direct solar heating and mechanically aspirated at all the NCAR and the CU towers and were naturally ventilated at the USGS tower to prevent the shelter heating effect on the measured temperature. The CME04 instrument deployment and challenges, as well as data issues, are described at the EOL Web site (www.eol.ucar.edu/cme04).

To investigate how mesoscale motions, such as mountain gravity waves and rotors, might affect our ability to scale up local CO_2 transport to a mountain region, the wind profile above the top of the towers was monitored by a Scintec flat array sodar (Scintec model MFAS). These data were collected from 10 May to 6 August 2004 every 10 min except between 2 and 7 June when they were collected every 15 min (Fig. 2). The sodar sampled the air volume within a cone of 22° from the vertical with the range gate of 10 m. Three-dimensional wind vector profiles were measured between 30 and 500 m above the ground, except during 10–11 May, when measurements were made between 30 and 600 m above the ground. In addition, the sodar measured vertical profiles of the standard deviation of three orthogonal wind components from more than 250–300 pulses during each 10-min sample interval, which provided unique information on the vertical distribution of turbulence intensity. Because of the motion of the surrounding trees, the sodar measurements below ~50 m were discarded. The wind speed uncertainty is 0.1–0.3 m s^{-1} for horizontal components and 0.03–0.1 m s^{-1} for vertical ones, and the wind direction uncertainty is 2°–3° depending on the sodar operation setting. The total number of acceptable wind measurements decreases with height because of the decreasing signal-to-noise ratio. Only 39% of the wind speed measurements reached 500 m above the ground in comparison to 94% at 100 m.

Since CO_2 transport was the focus of the ground field campaign, CO_2 concentration differences between locations were particularly important. To ensure an accurate CO_2 concentration measurement, a centralized CO_2 analyzer was placed at each of the three NCAR towers in addition to the ongoing CU and USGS CO_2 measurements (Table 2). Two Autonomous Inexpensive Robust CO_2 Analyzer (AIRCOA) systems (Stephens et al. 2006), which are modified LI-820 CO_2 infrared analyzers, were deployed: one at the willow site and the other at the aspen site. The NCAR trace gas measuring system (TGaMS), which is based on a LI-7000 infrared CO_2/H_2O analyzer, was deployed to collect air samples at 18 inlets for the vertical CO_2 profile at the pine tower and the horizontal variation of CO_2 concentration across Como Creek (Burns et al. 2006, 2009). The location and the height of CO_2 concentration measurements across Como Creek are provided in Table 3 and marked in Fig. 2. To measure the spatial variation of CO_2 concentration along Como Creek, two inlets were placed 1 m above the water level west and east of the cross-creek CO_2 sampling line. However, the TGaMS sampling buffer volume connected to the west inlet was found to be leaking toward the end of the experiment, so the west point data could not be used. A leaking problem also affected the CO_2 concentration measurement at 1 m above the ground 60 m south of the pine tower. Both the AIRCOA and TGaMS CO_2 measuring systems were equipped with four calibration gases, although early on not all four were used on TGaMS. We used two calibration gases for the CU and USGS CO_2 systems. The calibration gases at the CU and NCAR towers were tied to the World Meteorological Organization (WMO) standard scale through transfer calibration with an uncertainty of ±0.1 ppmv. All the CO_2 systems have a similar computer-controlled sampling strategy of periodically switching between observational inlets and calibration gases. Each measuring cycle (i.e., the time for the CO_2 analyzer to sample all the inlets) lasted from 6 min at the CU system to 30 min at the TGaMS system. The computer-controlled sampling system allowed us to easily modify the sampling frequency of any inlet during the experiment. For example, we could focus on the spatial variation of CO_2 concentration across

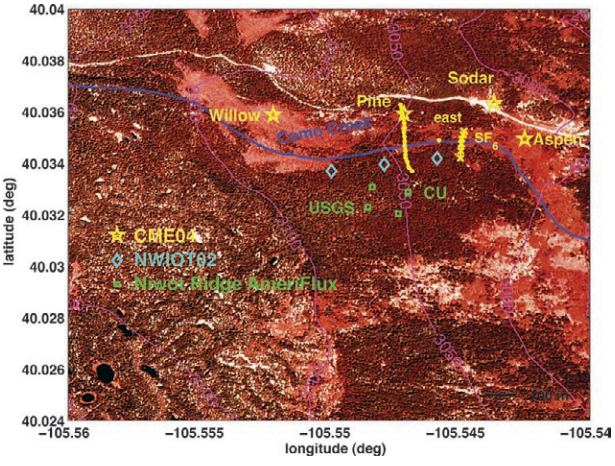

Fig. 2. The tower layout during CME04 (yellow) and NIWOT02 (light blue), and the existing Niwot Ridge AmeriFlux towers (green). The line south of the pine site marks the cross–Como Creek CO_2 measurements at various heights above the ground. The point on Como Creek marked "east" was the location of the CO_2 concentration measured 1 m above the water level. The sampling line for the SF_6 measurements is also marked.

or along Como Creek at any moment by sampling that subset of inlets more frequently. The quality control of the CO_2 concentration measurement and the intercomparison among the different CO_2 sampling systems during CME04 were discussed in detail by Burns et al. (2006, 2009).

Table 2. The existing facilities at the Niwot Ridge AmeriFlux site.

Z (m)	USGS				CU
	Main	ST	NT	CU	
33.0	*C*, *T*/RH, V_C, C′, R_{net}, R_{sw}, PAR				
25.5					R_{net}, PAR
23.0				*C*	
21.98					TC
21.5					*C*, *T*/RH, V_C, *C*′, *Q*
19.5					TC
16.5					TC
12.98					TC
12.5					*C*′, V_A, *Q*
12.0					P_2
10.0	*C*, *T*/RH, U			*C*	*C*
9.93					TC
8.06					TC
8.0					*T*/RH
6.0	*C*, U	*C*, U	*C*, U	*C*	
5.92					TC
5.7					V_C
5.0					*C*
3.96					TC
3.0	*C*, U			*C*	*C*
2.56					V_C, *C*′, *Q*
2.0	*T*/RH, V_C, *C*′				*T*/RH, TC
1.38					TC
1.0	*C*, U, P_1	*C*, U	*C*, U	*C*	
0.91					TC
0.5					C
0.4					TC
−15 to 0 cm					Q_{soil}, T_{soil}

All the symbols are the same as in Table 1, except that here

U = 2D Handar sonic by Vaisala.

P_1 = pressure measured with Vaisala model PTB101B.

TC = temperature measured with thermocouples built by NCAR.

Q_{soil} = soil moisture measured with Campbell CS615.

T_{soil} = soil temperature measured with REBS STP-1 platnium resistance thermometer

PAR = photosynthetically active radiation measured with a LI-190SA sensor at CU and a LI-190SZ sensor at USGS.

R_{sw} = downward solar radiation measured with a LI200 sensor.

T/RH = air temperature and humidity measured with Vaisala HMP35D, which is mechanically aspirated at CU, and naturally aspirated at USGS.

C = CO_2 concentration measured with a LI-6251 at CU and with a LI-7000 at USGS.

C′ = fast response CO_2 concentration measured with LI-6262 except at 2.56 m on the CU tower where LI-7500 was used.

To investigate the origin of the anticipated high CO_2 concentration, the flow pattern, and CO_2 dispersion over Como Creek at night, an SF_6 tracer study was conducted from 19 to 30 July 2004. During each nighttime experiment, the tracer from a single point near the surface along or to the side of Como Creek was released continuously at a steady rate. An automated horizontal sampling system, Trace Gas Automated Profile System (T-GAPS), was deployed to measure horizontal concentration profiles of both SF_6 and CO_2 across Como Creek at 1 m above the surface from several points ranging from 40 m north to 80 m south of the creek (Fig. 2). T-GAPS enabled the automated, continuous collection and analysis of simultaneous 5-min averaged samples from seven distributed inlets throughout each nighttime tracer release period (typically 1700 through 0500 LST). For a short period, SF_6 was also measured through TGaMS.

Airborne Carbon in the Mountain Experiment. A total of 16 flights were conducted with the NCAR C-130 aircraft during ACME04 over the Colorado Rocky Mountains (Table 4). The goals of the airborne campaign were 1) to investigate whether we could observe the transport of the respired CO_2 by morning mountain circulations, which contributes to the disappearance of the cold CO_2 pools accumulated at night; 2) to examine the feasibility of CO_2 budget methods to obtain regional surface CO_2 fluxes over mountainous terrain and their seasonal variation; 3) to distinguish biogenic from anthropogenic carbon sources using an isotope analysis; and 4) to characterize changes in surface–atmosphere carbon exchange following a large forest fire. To investigate the pattern of morning CO_2 venting by the mountain wind circulation, a "racetrack" flight pattern was designed to measure the spatial variation of CO_2 concentration and CO_2 fluxes adjacent to the mountain peaks and valleys at about 0600–0700 LST. The approximately oval racetrack consisted of a west leg at a constant flight level passing over the

Table 3. TGaMS measurement heights and locations across Como Creek*.

D (m)	Height above the ground (m)		
	7 Aug–9 Sep	9–17 Sep	17 Sep–5 Oct
–20	1	None*1	None
0 (pine)	1	1, 4	1 and 4
20	1	1	None*6
40	1	2*2	None*7
60	1	1	1
80	1	None*3	None
100	1	4*4	4
120	1	None*5	None
140	1	0.2, 0.5, 1	0.2, 1, 4*8
160	1	4*4	4
180	1	1	1
220	None	None	4
260	None	None	1

D = the distance of each inlet from the pine tower, where positive represents south of the pine tower.

* Some inlets across Como Creek were moved twice: 9 Sep and 7 Aug. The table here shows the location of each inlet during the three periods.

*1 The inlet was moved to 4 m at the pine tower.

*2 The inlet was moved from 1 to 2 m at the same location.

*3 The inlet was moved to 0.2 m at *D* = 140 m.

*4 The inlet was moved from 1 to 4 m at the same location.

*5 The inlet was moved to 0.5 m at *D* = 140 m.

*6 The inlet was moved to 1 m at *D* = 260 m.

*7 The inlet was moved to 4 m at *D* = 220 m.

*8 This inlet was moved from 0.5 m at the same location.

CME04 site ~10 km east of the mountain peaks of the Rocky Mountain Front Range, an east leg about 15 km east of and 500 m below the west leg, and south and north legs connecting the west and east legs (Fig. 1). The racetrack was flown consecutively 2–3 times to increase the turbulent flux samples. After each racetrack, a "roller coaster" track was flown to sample the spatial variation of CO_2 concentration along the mountain slope. In addition, we collected air samples from the C-130 and analyzed the stable isotope content of CO_2 to provide some insights into regional flux dynamics. The stable isotope content of CO_2 provides information about the photosynthetic and respiratory origins of near-surface CO_2. To examine the feasibility of calculating the regional CO_2 flux using the CO_2 budget method, its seasonal variation, and the controlling variables for the regional NEE in this mountainous terrain under fair weather conditions, we used a Lagrangian approach to infer the areal CO_2 surface fluxes over the western Colorado mountains. The CO_2 concentrations of the air mass before it enters the domain and after it exists the domain with the influence of the CO_2 source/sink within the domain were measured in the morning and afternoon. The location and the timing of these profiles were estimated using several forecast models and the Stochastic Time Inverted Lagrangian Transport (STILT) model before each flight (Lin et al. 2003). To cover the seasonal variation of the ecosystem–atmosphere carbon exchange, three 2-week field campaigns were designed to cover the period between spring and fall. To distinguish

Table 4: ACME04 C-130 flight summary.

Flight No.	Date	Time (LST)	Flight pattern	Weather (m s^{-1}, °)*
RF01	14 May	0553:52–0934:00	ST at NP & Rangely, MA at KR. RT, RC	20, 270
RF02	14 May	1247:35–1355:59	East of CME04	22, 270, cloudy
RF03	20 May	0529:16–0913:10	ST at NP and Montrose, MA at KR. RT, RC	30, 240, cloudy
RF04	20 May	1131:30–1341:30	ST at NP & Glennwood Springs	18, 220, cloudy
RF05	27 May	0530:17–0910:50	ST at NP & Greystone, MA at KR. RT, RC	30, 270
RF06	28 May	1300:00–1512:45	ST at NP & KR. RT, RC, MA at Centennial	20, 240, cloudy
RF07	12 Jul	0531:01–0901:43	ST at NP & KR. MA at KR. RT, RC, ST at Granby-Avon	8, 270, cloudy
RF08	12 Jul	1132:55–1504:10	ST at NP, KR, & Granby. RT, RC. ST at CME04	8, 270, cloudy
RF09	20 Jul	0532:54–0856:00	Hayman, ST at Avon-Leadville-Salida, RC, RT, MA at Centennial	8, 300
RF10	20 Jul	1234:10–1500:00	Hayman, ST at Avon-Leadville-Salida, RT	8, 270, cloudy
RF11	22 Jul	0537:00–0917:46	MA at KR. ST at CME04, Indian Meadows, RMNP, NP, Hayden. RC, RT	8, 270
RF12	26 Jul	0539:24–0855:00	ST at NP & Granby, MA at KR. RC, RT	12, 300
RF13	26 Jul	1223:01–1441:05	ST at NP, Granby & CME04, RT, RC	8, 300
RF14	29 Jul	0549:00–1107:00	ST to Rock Springs, Rifle, Avon, Fairplay. MA at KR & Hayden RC, RT	18, 270
RF15	29 Jul	1301:00–1421:00	ST to Laramie & Glendevey, CME04. RC	18, 290
RF16	2 Aug	0808:10–1238:00	MA at KR & LE. RT, cross-divide loops	8, 270, scattered clouds

ST = saw tooth.

RT = racetrack over CME04.

RC = roller coaster.

MA = missed approach.

NP = North Park, Colorado.

RMNP = Rocky Mountain National Park, Colorado.

LE = Leadville, Colorado.

KR = Kremmling, Colorado.

* at approximately 5000 m above sea level right after the C-130 took off.

fossil fuel derived from biogenic CO_2 emissions, we analyzed the air samples for radiocarbon isotope content of CO_2 (Graven et al. 2009). To investigate the effect of forest fire on ecosystem–atmosphere carbon exchange, we flew over an undisturbed healthy forest and the forest recovering from the 2002 Hayman fire (see en.wikipedia.org/wiki/Hayman_Fire).

On board the NCAR C-130 aircraft, the standard in situ meteorological variables, such as wind, temperature, humidity, and downward and upward longwave and shortwave radiation, were measured (www.eol.ucar.edu/instrumentation/aircraft/C-130/documentation/c-130-investigator-handbook). In addition, in situ CO and CO_2 concentrations were measured by an Aero-Laser AL5002 instrument and a modified nondispersive infrared (NDIR) CO_2/H_2O absorption analyzer (LI-6262), respectively. The CO concentrations were used as a tracer for identifying anthropogenic CO_2 emissions. The CO vacuum UV resonance fluorescence instrument is functionally similar to that of Gerbig et al. (1999). The CO data have a 3-ppbv precision, 1-s resolution, and a typical accuracy of ±10% for a 100-ppbv ambient mixing ratio. The CO_2 sensor was modified to implement temperature and pressure control after the Earth Resources-2 (ER-2) instrument described by Daube et al. (2002). Since the CO_2 sensor was developed for lower tropospheric measurements, humidity was removed from ambient air prior to analysis using a single Nafion semipermeable membrane dryer (Perma Pure LLC) followed by passage through a low-volume, dry ice–cooled cryogenic trap. The CO_2 data have a 1-s time resolution and a precision and accuracy of ±0.3 ppmv for a 10-s averaging time. The CO_2 concentration was periodically calibrated with four calibration gases (355, 373, 390, and 395 ppm) for all the flights. Both in situ CO and CO_2 concentrations were measured at 25 Hz and averaged to 5 Hz. In addition to the onboard in situ measurement, the NCAR Multichannel Cloud Radiometer (MCR) with seven channels was also flown aboard the NCAR C-130 to remotely observe ground features such as the normalized difference of vegetation index (NDVI) and surface radiation temperature (Fig. 3). Its swath was about twice the aircraft height above the ground.

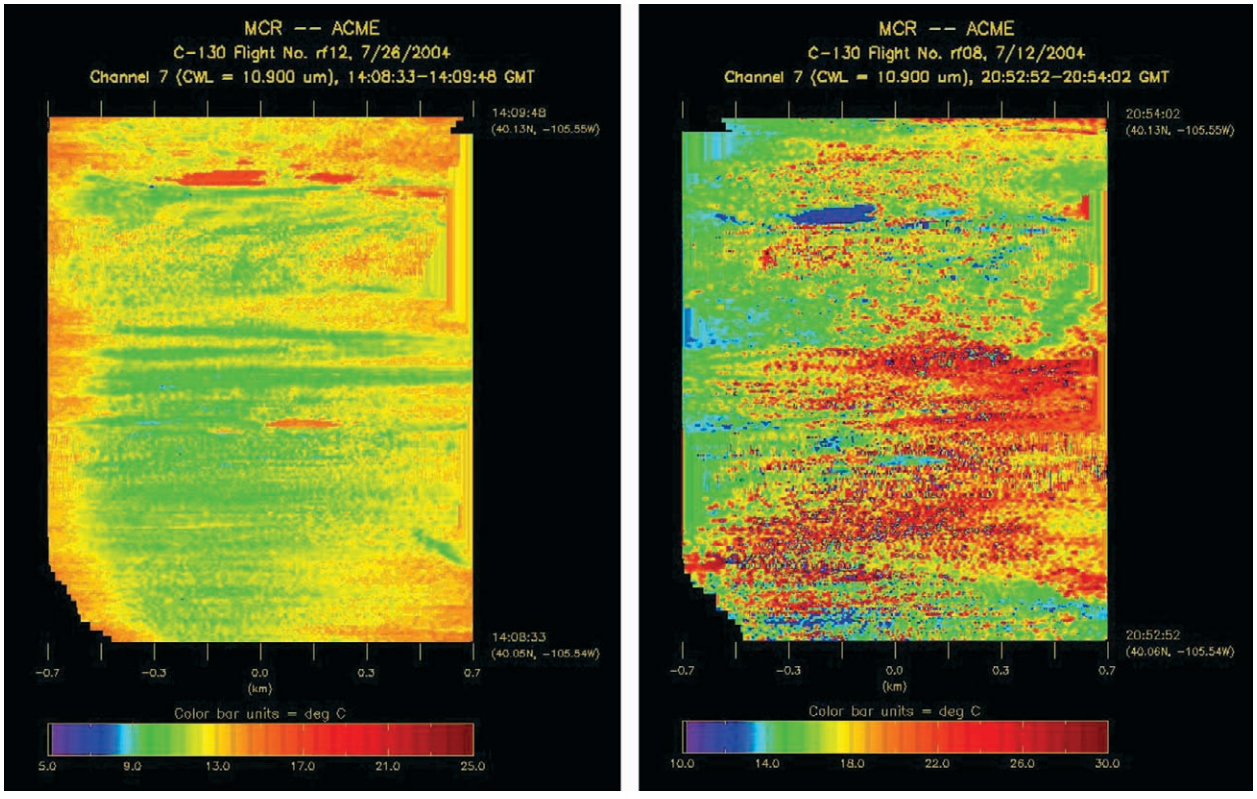

Fig. 3. The surface radiation temperature measured by the NCAR MCR (left) in the morning of 26 Jul and (right) in the afternoon of 12 Jul over the area north of the CME04 site. The two images capture the diurnal variation of the surface temperature over heterogeneous surfaces, where water bodies (the red spots at the top of the left image) were warmer than ground surfaces (green areas on the left image) at night and colder (the blue spots on the right image with the same shapes as the red spots on the left image) during the day.

Ground and airborne isotope observations. The oxygen and carbon isotopic composition of atmospheric CO_2 is affected by metabolic and physical discrimination against different isotope forms and therefore is a useful proxy for assessing those processes involved in surface–atmosphere CO_2 exchange (Ciais et al. 1995; Fung et al. 1997; Scholze et al. 2003; Schaeffer et al. 2008; Bowling et al. 2008). During our field campaign, the isotope observations were used for the following purposes: 1) to understand elevational variation of nighttime-respired CO_2; 2) to investigate whether the morning upslope winds, which develop as the eastern slope of the mountains heat up, are partially responsible for the disappearance of the nighttime accumulated CO_2 pool at downslope accumulation sites by transporting the CO_2 to regions aloft; and 3) to identify the biogenic/anthropogenic CO_2 origin.

In addressing the first goal, we assumed that the ^{18}O content of soil respired CO_2, which is expressed as $\delta^{18}O$ (Fry 2006), would be determined by exchange with soil water in the vicinity of the respiration source. The ^{18}O of soil water varies with elevation; thus, the ^{18}O of respired CO_2 could provide information on both the respiration rate and the elevational range within which the CO_2 was respired. We attempted to understand the $\delta^{18}O$ spatial pattern of soil and plant water by collecting three soil samples from 0 to 10 cm below the ground and five stem samples at each of 16 sites along an altitudinal gradient of 1750–3390 m above sea level in an area of 1.3–28 km northwest to northeast of the CU tower in September 2005. We then examined the relationship between the $\delta^{18}O$ values of the soil-respired CO_2 and of soil and plant water by collecting three CO_2 samples, five decorticated stem samples, and three soil cores at each of 14 sites along an altitudinal gradient from 1721 to 3319 m above sea level in an area of 1–30 km northwest to northeast of the CU tower during August 2007. The soil cores were separated into three samples representing different soil depths: 0–10, 10–25, and 25–40 cm. The CO_2 samples were collected in 2-L flasks using a pump system to circulate air from the soil chamber to the flask. The entire chamber and flask system were first scrubbed of CO_2 to 0–5 ppm and water vapor to 0 ppm before collecting a CO_2 sample, which had a mean concentration of 394 ± 10 ppm. Water from all the soil and stem samples was distilled by cryogenic distillation (Vendramini and Sternberg 2007). Oxygen and hydrogen isotope ratios were measured at the Laboratory for Stable Isotope Ecology in Tropical Ecosystems (LSIETE) at the University of Miami (Miami, Florida) by equilibrating each sample with either carbon dioxide or hydrogen, respectively. The CO_2 vessels were sent to the Institute of Arctic and Alpine Research (INSTAAR; Boulder, Colorado) for the isotopic analysis of carbon and oxygen isotope ratios after correction for nitrous oxides.

To achieve our second goal, which was to study the isotope signal for identifying the accumulated nighttime CO_2 trapped in valleys and transported by the morning upslope flow, we collected air samples within and above the canopy at two locations within 100 m of the CU tower and aboard the C-130 aircraft. The air samples were collected with 100-mL glass flasks (Kontes Glass Co., Vineland, New Jersey) to analyze CO_2 concentration and $\delta^{13}C$ and $\delta^{18}O$ of the atmospheric CO_2 (Schauer et al. 2003; Lai et al. 2006). Two programmable flask samplers controlled by CR23X data loggers (Campbell Scientific, Logan, Utah) were used to fill flasks on the ground. One sampled at 15-min intervals during the night before each morning flight. The other started sampling approximately 2 h before each afternoon flight and continued throughout the flight. For comparison with the ground measurement, air samples were also collected aboard the C-130 aircraft in the early morning (~0700 LST, about 2 h after sunrise) for comparison with the ground measurement using a customized sampling unit, which allows for 16 flask collections per flight. The air sample was drawn from an inlet free from the engine exhaust and predried by flowing through a magnesium perchlorate trap (120 mL) at a constant flow rate of 3.3 L min^{-1} and flask pressure of 100 kPa. The flasks were flushed for at least 20 s (median time = 2.4 min) before filling. A total of 524 flasks were collected for stable isotope analysis during ACME04. All flask air samples were analyzed at the Stable Isotope Ratio Facility for Environmental Research (SIRFER) at the University of Utah. The CO_2 concentration and isotope ratios were measured with an automated continuous-flow isotope ratio mass spectrometry (CF-IRMS) system (Schauer et al. 2005). The CO_2 concentration measurements were traceable to a WMO standard scale using CO_2 primary cylinders (ranging from 217 to 526 ppm) certified by the Earth System Research Laboratory at the National Oceanic and Atmospheric Administration. Schauer et al. (2005) reported precisions of 0.06‰, 0.11‰, and 0.32 ppm for $\delta^{13}C$, $\delta^{18}O$, and CO_2 concentration, respectively, with two replicate injections. We doubled the number of replicates when analyzing airborne air samples, and consequently we improved the precision to 0.05‰, 0.08‰, and 0.16 ppm for $\delta^{13}C$, $\delta^{18}O$, and CO_2 concentration, respectively.

To achieve our third goal, which was to distinguish biogenic from anthropogenic CO_2 emissions, we

analyzed the ^{14}C or radiocarbon signal of the atmospheric CO_2. Because fossil fuel–derived CO_2 contains no ^{14}C, it is a sensitive tracer for anthropogenic influence on CO_2. The air samples for the ^{14}C analysis were collected aboard the C-130 aircraft during its vertical profiling of the lower troposphere in rural and urban areas of Colorado in May and July 2004. The measurement details were described in Graven et al. (2009).

FIELD EXPERIMENT RESULTS. *Preliminary results from the ground field campaign.* By analyzing the spatial variation of the CO_2 concentration measurements during CME04, we confirmed a dominant role for Como Creek in channeling the nighttime accumulation of respired CO_2. We observed that the monthly averaged CO_2 concentration was often high over Como Creek although the highest concentration section tended to fluctuate with time, often developing on the north side of the creek at the beginning of each night and moving toward the center of the creek channel by the early morning (Fig. 4). We speculate that the drift is associated with asymmetric slopes along the two banks of the creek, which forced the pattern of cold-air drainage to not exactly coincide with the creek channel. In addition, we found that the drainage air was not uniformly high in CO_2 concentration across Como Creek; that is, the CO_2-rich air was concentrated in patches or "blobs," which was subsequently confirmed by Oncley et al. (2009) using a tram system with a moving CO_2 sensor that crossed Como Creek every 90 s. The vertical CO_2 profiles sampled at 0.2, 0.5, and 1 m above the ground next to Como Creek and within 15 min of each other from 9 to 17 September 2004 indicated that the CO_2 concentration did not consistently decrease with height at night, as we might expect in the presence of a stable boundary layer. Instead, it sometimes increased with height and sometimes had a minimum concentration at 0.5 m, which reflected the transient character of the CO_2-rich air patches. Close to the ground at night, we found that the temporal variation of the CO_2 concentration was approximately inversely related to oscillations in wind speed; however, in contrast to the result of Doran and Horst (1981), no particular oscillation frequency was found. The relationship between the patchy character of the CO_2-rich air and wind speed variation will be further investigated.

Spatial variability in the CO_2 concentration across Como Creek and its associated footprint were investigated through the SF_6 tracer study, with the tracer releasing approximately 200 m upstream of the sampling sensor array that stretched across Como Creek (Fig. 5). The spatial variations of both SF_6 and CO_2 concentration across Como Creek suggest that respired CO_2 drains from valley slopes toward the creek to produce somewhat elevated CO_2 concentration along the creek. The SF_6 crosswind concentration profile was integrated horizontally with an assumed Gaussian vertical distribution and combined with measured downslope wind speeds to yield an estimate of the mass flow rate of the tracer through the vertical sampling plane across the creek. This process showed relatively good agreement with the SF_6 release rate.

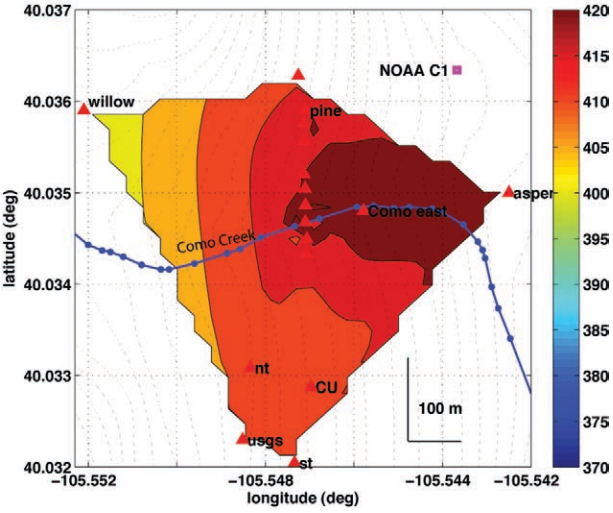

FIG. 4. The spatial distribution of CO_2 concentration (in ppm) at 1 m above the ground composited between 28 Aug and 7 Sep at 0300 LST. The red triangles mark the inlets for the CO_2 measurement 1 m above the ground during CME04.

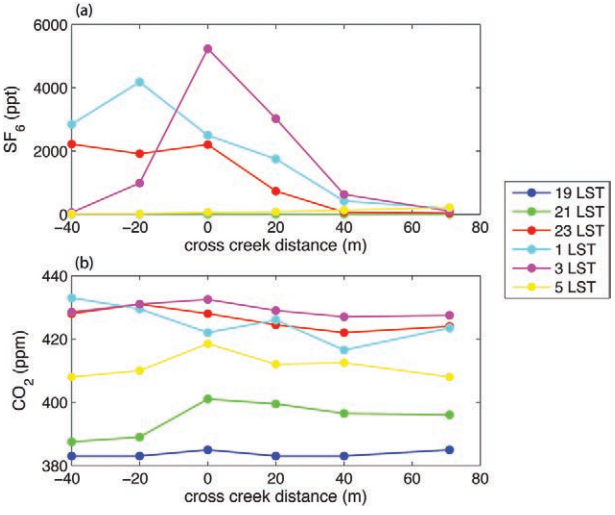

FIG. 5. The hourly averaged, cross-Como-Creek-flow concentration profiles of (a) SF_6 and (b) CO_2 at 1 m above the ground along the sampling line indicated in Fig. 2 during the night of 27–28 Jul. The positive distance represents the distance south of Como Creek.

The same approach was used with the CO_2 crosswind concentration distribution and an estimate of the CO_2 soil respiration rate to estimate an upwind fetch contributing to CO_2 draining into the Como Creek channel. This calculation produced an estimated fetch of approximately 500–600 m for CO_2 surface fluxes contributing to the downslope atmospheric CO_2 concentration measured at the sampling array across Como Creek.

Using the sodar data, we found that the wind speed aloft often oscillates (Fig. 6b) and the intensity of the vertical velocity fluctuation increases with wind speed when buoyancy is not strong, as shown in Fig. 6d. Because the vertical direction of the sodar is aligned parallel to gravity rather than perpendicular to the local slope, part of the along slope flow fluctuation is reflected in the vertical wind fluctuation measured by the sodar. In addition, the relatively large sample volume of the sodar measurement may cover the large inhomogeneous turbulent domain. As a result, we found that the standard deviation of the vertical velocity measured by the sodar does not decrease significantly as wind speed decreases. The wind speed between the sonic at 30 m on the aspen tower and the sodar measurement at 50 m above the ground was, on average, within 1 m s^{-1} despite the difference between their sampling volume and separation distance of ~300 m.

In making the transition from the local carbonshed to regional scales, we used the isotopic composition for CO_2 to discern elevational patterns in the redistribution of respired CO_2. We observed no discernable altitude-dependent $\delta^{18}O$ values of stem water. However, the $\delta^{18}O$ value of soil water at 0–10-cm depth was highly correlated with altitude ($P < 0.0001$, $R^2 = 0.80$), and larger at lower elevation (Fig. 7a). The range of the $\delta^{18}O$ value, about 12.5‰, was much greater than the expected value of ~3.1‰, which is predicted based on the simple Rayleigh distillation effect (i.e., heavy isotopes condense faster than light ones during precipitation) with consideration of the observed latitude and altitude variation of the air temperature using the Bowen–Wilkinson equation (Bowen and Wilkinson 2002). The observed hydrogen

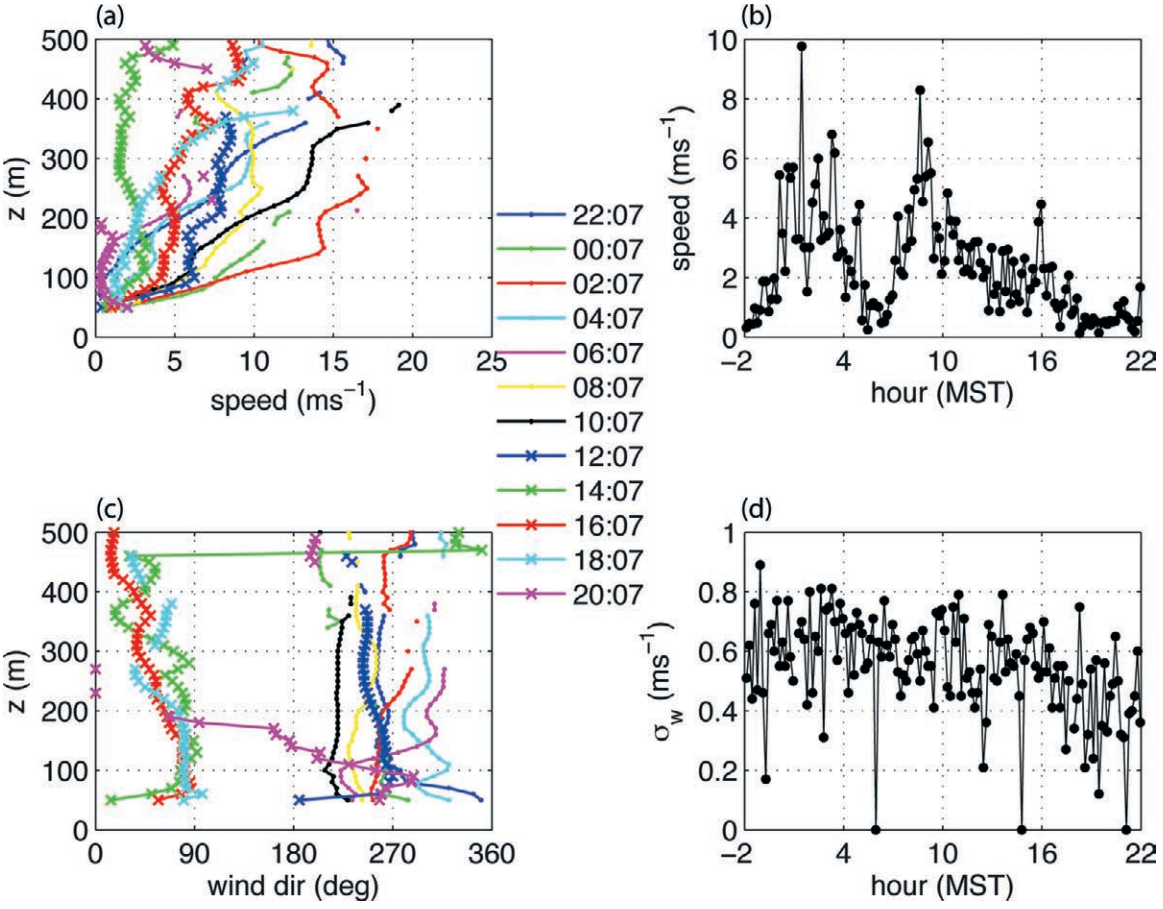

Fig. 6. The vertical profiles of (a) wind speed and (c) wind direction every 2 h (LST); (b) the time series of the horizontal wind speed; and (d) the standard deviation of the vertical velocity σ_w at 70 m above the ground measured by the sodar on the night of 18–19 May 2004.

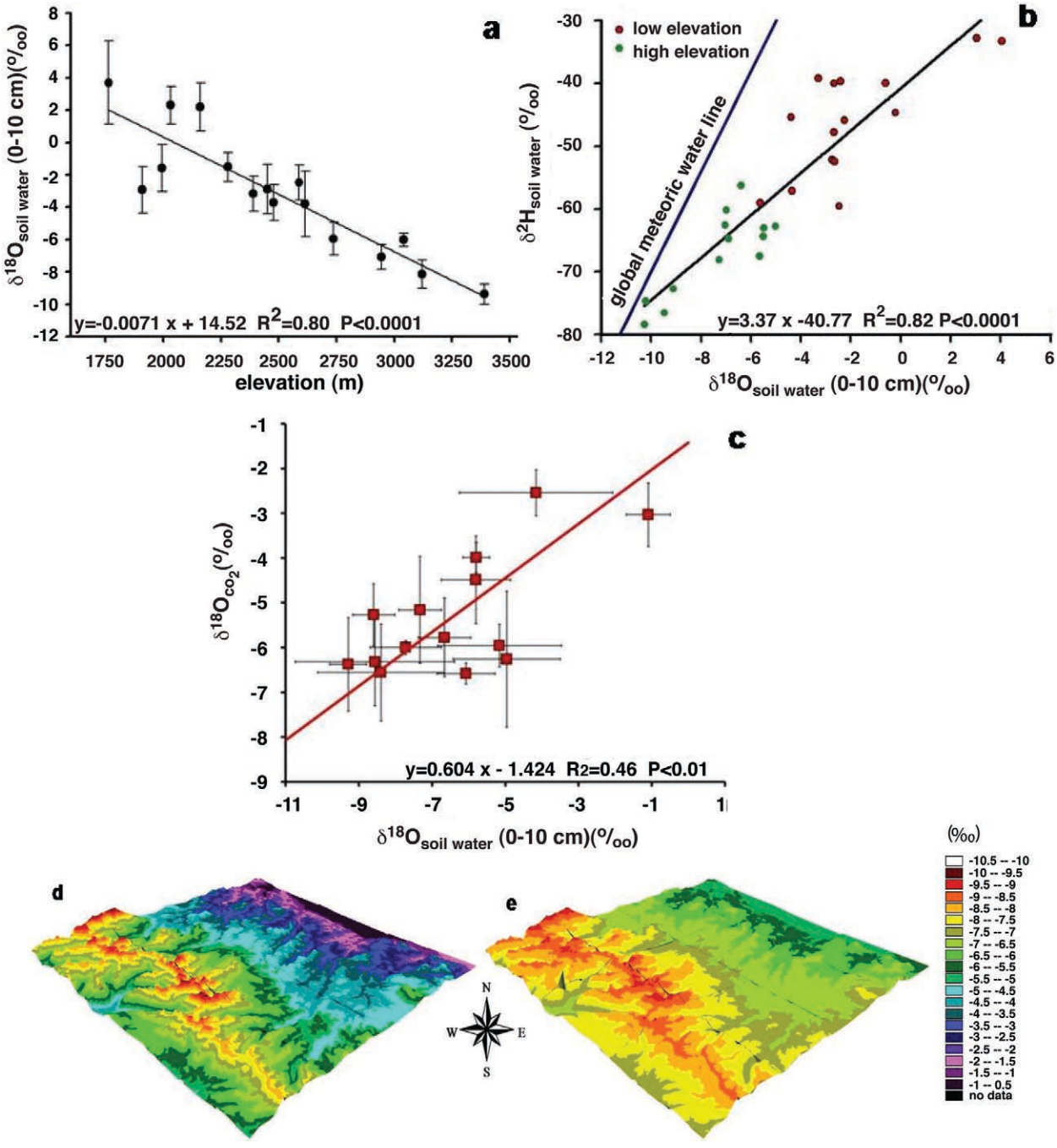

FIG. 7. (a) The soil water samples collected from 0 to 10 cm in 2005 over an altitudinal gradient of 1640 m (1750–3390 m). Each data point is the mean of three soil samples, and standard error bars are shown for $\delta^{18}O$ of soil water. (b) $\delta^{2}H$ versus $\delta^{18}O$ plot for soil samples collected in September 2005. The blue line represents the global meteoric water line [$\delta^{2}H = 8(\delta^{18}O) + 10$]. All of the soil water samples fall to the right of the global meteoric water line, which indicates that the soil water was undergoing evaporative enrichment, especially at lower elevations. (c) The $\delta^{18}O$ of CO_2 versus $\delta^{18}O$ of soil water at 0–10 cm collected in August 2007 and the regression line. Standard error bars are shown for both $\delta^{18}O$ of CO_2 and $\delta^{18}O$ of soil water. (d) A GIS map of the predicted $\delta^{18}O$ of CO_2 based on the empirical relationship among $\delta^{18}O$ of soil-water, elevation, and soil-respired CO_2 developed at the site. (e) A map of the expected $\delta^{18}O$ values of CO_2 based on the equilibration between soil-water and soil-respired CO_2, where the $\delta^{18}O$ value of the soil water is calculated from the $\delta^{18}O$ value of precipitation from the Bowen–Wilkinson equation with a constant evaporative enrichment value. Both maps are draped on a 3D elevation map. The coordinates for the corners of the study area are 40.248°N, 105.751°W; 40.248°N, 105.251°W; 39.875°N, 105.751°W; and 39.875°N, 105.251°W. Comparison of (d) and (e) indicates that as a result of evaporation as a function of altitude, the range of oxygen isotope ratios of soil-respired CO_2 across the altitude gradient is much greater than expected.

(δ^2H) and oxygen ($\delta^{18}O$) isotopes in soil water all fall to the right of the global meteoric water line (Fig. 7b), suggesting that the greater-than-expected range of the $\delta^{18}O$ value across this altitudinal gradient is due to soil evaporation (Craig 1961). Soil evaporation, which has kinetic isotopic effects in addition to equilibrium effects, causes a disproportionate enrichment of $\delta^{18}O$ compared to δ^2H in the remaining water body. This effect skews the δ^2H versus $\delta^{18}O$ relation of evaporated water to the right of the global meteoric water line as observed. The departure of the observation from the global meteoric water line in Fig. 7b implies that the soil evaporation increased with decreasing elevation. The $\delta^{18}O$ value of soil-respired CO_2 was best correlated with the $\delta^{18}O$ value of the soil water from 0–10-cm depth (Fig. 7c).

Although soil-respired CO_2 approximately equilibrates with soil water at 0–10-cm depth before it is released into the atmosphere, the equilibration is not complete because the observed slope of the regression of $\delta^{18}O$ in soil-respired CO_2 versus that of soil water was less than 1. This less-than-expected slope could be caused by entrainment of atmospheric CO_2 into the upper layer of the soil, followed by incomplete isotopic equilibration with soil water (Miller et al. 1999). Based on the observed relationships in Figs. 7a and 7c, we mapped the expected $\delta^{18}O$ values of soil respired CO_2 across Niwot Ridge (Fig. 7d) and compared it with the map of $\delta^{18}O$ values of soil-respired CO_2 based on the Bowen–Wilkinson prediction with a constant offset for isotopic enrichment of soil water by evaporation (Fig. 7e). The large range in $\delta^{18}O$ values of respired CO_2 along the slope may be used to trace CO_2 transport from higher to lower elevations across the scale of the Rocky Mountain Front Range.

Preliminary results from the airborne campaign. Flying the racetrack at ~0700 LST for nine flights during ACME04, we investigated the effect of the upslope flow in bringing up the CO_2-rich air from the nighttime CO_2 pools. We found that under weak synoptic wind conditions (e.g., flight 11), the thermally forced upslope flow was evident from the easterly wind on the lower-elevation east leg, while the wind on the higher-elevation west leg was still northwesterly (Fig. 8). Because the west leg was about at the same altitude as the mountain peaks west of the leg, the northwesterly flow there could be a combination of the synoptic flow and the return flow as part of the upslope circulation constrained by mass conservation. The observed large variance of all the atmospheric variables on the west leg compared to that on the east leg indicates turbulence activity on the west leg and stable stratification at the east leg. Whiteman (2000, pp. 150 and 172) showed that when a shallow morning upslope flow reaches a mountain peak, the ascending flow induces descending motions (or oscillations, depending on the atmospheric stability) because of mass conservation. The stable air on the east leg may reflect the enhanced atmospheric stability from the sinking motion as part of the return flow bounded by mass conservation as well as the stable cold CO_2-rich air that formed during the previous night. The turbulence at the west leg may be generated by the convective activity at the top of the mountain peaks upstream of the west leg as well as the upslope flow. The smaller CO_2 concentration on the west leg compared to the east leg may reflect the CO_2 decrease with height as a result of the nighttime accumulation at lower elevation as well as a reduction from the local convective mixing in spite of the upslope transport of CO_2-rich air from lower elevation. The hypothesis on the role of the upslope flow on the CO_2 mixing along the mountain slope is supported by the almost identical $\delta^{13}C$–CO_2 concentration relation from both the air samples collected at the CME04 site before each morning flight and adjacent to the mountain peaks by the C-130. Figure 9 shows that in the early morning, CO_2 concentration and $\delta^{13}C$ of CO_2 were stratified

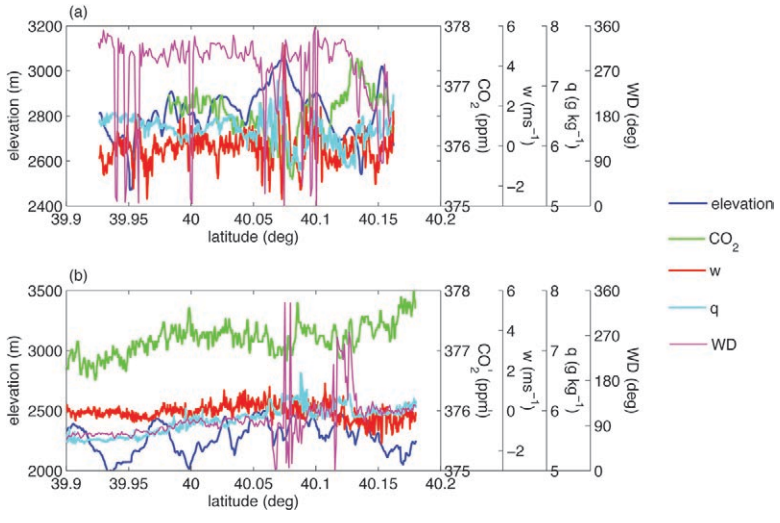

Fig. 8. The terrain elevation, CO_2 concentration, vertical velocity *w*, specific humidity *q*, and wind direction WD observed (a) along the west leg of the racetrack and (b) along the east leg around 0700 LST 22 Jul.

in the atmospheric boundary layer. As the morning progressed, the upslope flow mixed high CO_2 concentration and low $\delta^{13}C$ values of the surface air with lower CO_2 concentration and high $\delta^{13}C$ values of the upper boundary layer. The mixing is characterized as the linear relationship between CO_2 concentrations and $\delta^{13}C$ values, or the almost identical slopes of the linear regression lines between $\delta^{13}C$ and CO_2 concentration (−0.045 versus −0.043 ‰ ppm^{-1}) based on the data collected from the ground and the aircraft. All of this evidence can be used to suggest that the higher degree of spatial variation of CO_2 concentration above the mountain peaks may indeed be associated with the morning venting of CO_2-rich air from widely dispersed "pools" of high CO_2 that accumulated the previous night somewhere below as we hypothesized and as the atmospheric modeling work demonstrates (see next section). If much of this CO_2-rich air originated from the Denver metropolitan corridor and the eastern plains, which lie at the base of the mountains that the C-130 traversed, then our results suggest that mountain circulation patterns may draw biogenic and anthropogenic CO_2 upslope into the atmosphere above the mountains. Compensating descending air around the mountain peaks may reduce the boundary-layer growth rate and delay the convective mixing of CO_2 in the surrounding region.

Based on our observed CO_2 profiles on 29 July 2004, we found that the cold CO_2-rich pools of air within valleys were much deeper and persistent than those over relatively open areas—for example, see the comparison between the dark blue (over open areas) and the other profiles (within valleys) in Fig. 10. This agrees with observations in the literature (Whiteman 2000) of cold-air pools in many mountain valleys where a rapid early morning breakup is prevented by sinking motions over the valley center that stabilize the valley atmosphere. As a result of turbulent mixing after the ground was heated, the CO_2 concentration became vertically well mixed within the active mixing layer, as demonstrated in the relatively constant CO_2 concentration and potential temperature within the lowest 200 m (e.g., the green profile in Fig. 10). Because of the uptake of CO_2 as a result of ecosystem photosynthesis at the ground, the CO_2 concentration sometimes increased with height to the top of the mixing layer and decreased with height above (see the red and black profiles in Fig. 10), indicating that the CO_2 mixing and uptake under the deep CO_2 pool accumulated at night. By applying the unique technique of the $\Delta^{14}C$ analysis for air collected from the C-130, the observed high CO_2 pool in mountain valleys was found to be of biogenic origin (Graven et al. 2009). During each flight, we observed seasonal variations and the imprint of diurnal variations of regional photosynthesis in the CO_2 concentrations above 2000 m from the C-130, which indicates that fast (diurnal) and slow (seasonal) time scales are involved in producing the CO_2 concentration in the lower troposphere (Fig. 11).

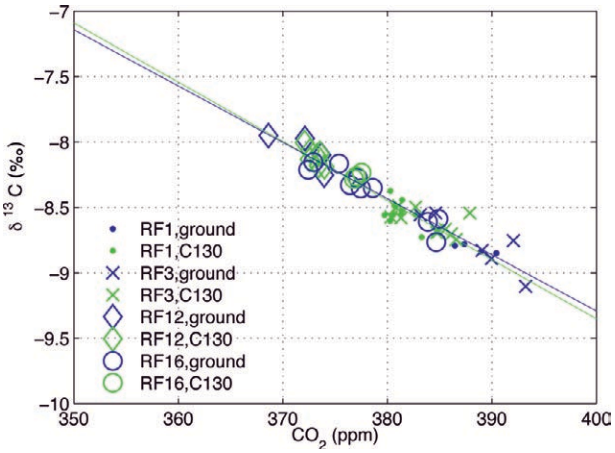

Fig. 9. Comparison of the CO_2–$\delta^{13}C$ relationship between the aircraft flask measurements during the morning racetrack flights and the ground flask measurements collected before those flights during ACME04. The green and blue lines represent the linear regression lines for the aircraft and ground measurements and have slopes of −0.045 and −0.043‰ ppm^{-1}, respectively.

PRELIMINARY MODELING RESULTS. *Spatial distributions of CO_2 concentration over the Rockies.* To understand the CO_2 observations from CME04 and ACME04 and in an attempt to estimate regional carbon uptake, a mesoscale model based on the Regional Atmospheric Modeling System (RAMS; Pielke et al. 1992) was used to simulate CO_2 transport. We used a simple sinusoidal pattern to represent the diurnal variation of the surface CO_2 flux and initial CO_2 concentrations based on observed NEE and CO_2 concentration taken from the CU tower measurements. These patterns were then used with RAMS to simulate the CO_2 transport on 12 July 2004. The model was run at 1.5-km horizontal resolution for the domain of the ACME04 field campaign.

In the morning shortly after sunrise, cold-air pools were simulated to be present in the valleys (Fig. 12a), coinciding with the CO_2-rich air pools that we observed at night (Fig. 12b). The simulation also shows that cold CO_2-rich air in the valleys can persist for hours after sunrise and only become vertically well mixed near noon, which is consistent with what we observed using our airborne measurements. In the afternoon, surface

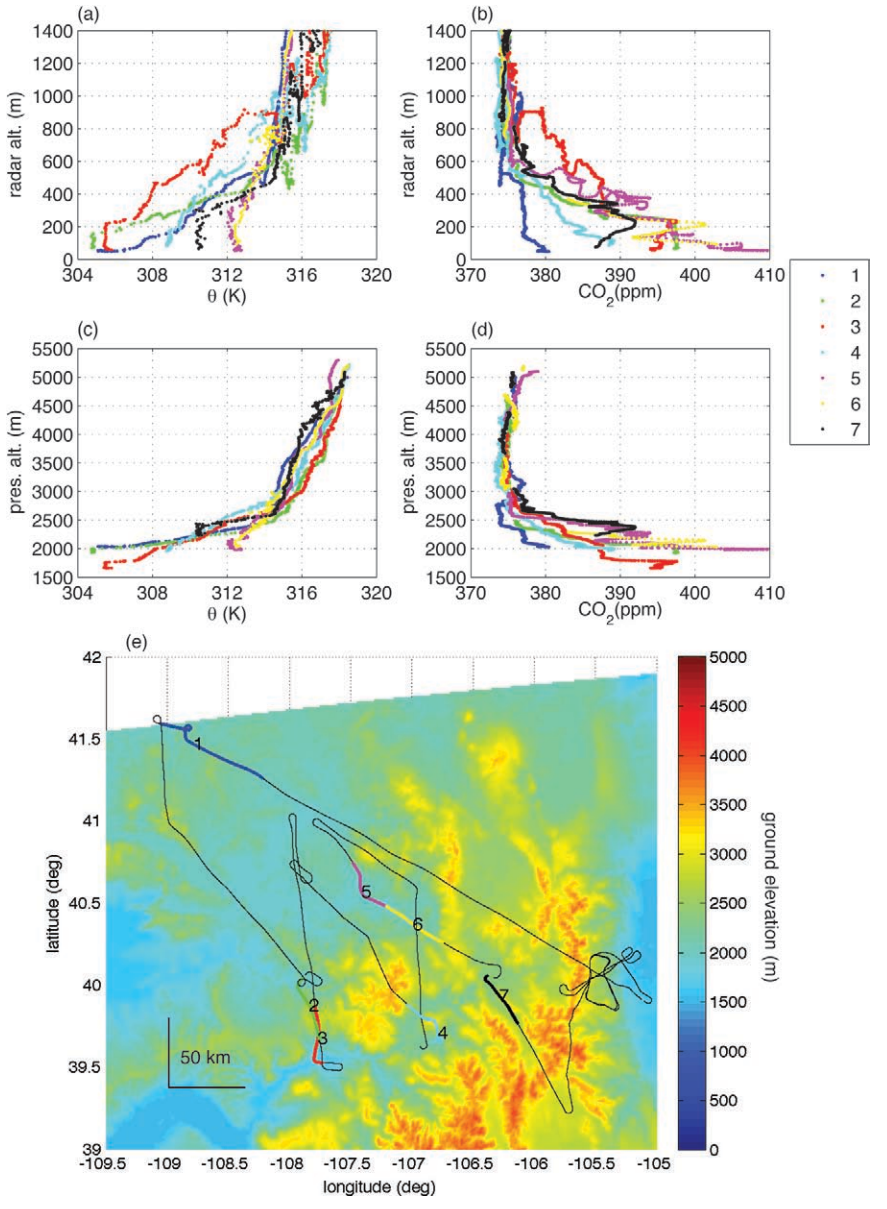

Fig. 10. The vertical aircraft potential temperature θ and CO_2 profiles from flight 14 on 29 Jul 2004 as functions of (a),(b) altitude above the ground (radar altitude) and (c),(d) altitude above sea level (pressure altitude). (e) Locations marked with the same colors and numbers as in (a)–(d).

heating leads to a well-mixed boundary layer (Fig. 12c). Continuous photosynthetic CO_2 uptake, which was included in the model as imposed CO_2 exchange at the bottom of the domain, caused a decrease in the simulated CO_2 concentration of the lower atmosphere (Fig. 12d). The subsequent horizontal and vertical transport of CO_2 by thermally driven slope and valley flows led us to predict a complex spatial structure in the CO_2 concentration with large horizontal CO_2 gradients within and above the deep boundary layer over the mountains during the daytime. A large spatial variation of CO_2 concentration is found close to the ground at night, but it extends to the entire atmospheric boundary layer during day. Plumes of air with low CO_2 concentration were sometimes observed well above the height of the mountains during the day. The simulated diurnal transport of CO_2 qualitatively resembled our observations, which confirmed the role of the thermally driven mountain circulation and the boundary layer evolution over complex terrain in regional ecosystem–atmosphere carbon exchange. However, the strength of the mountain circulation seems to be overestimated in the model and the ecosystem–atmosphere carbon exchange is oversimplified.

Regional surface CO_2 flux using the CO_2 budget method. We applied a CO_2 budget method using our aircraft profile observations to retrieve regional CO_2 fluxes over a domain covering a large part of the Colorado Rockies. The CO_2 concentrations of an air mass before it entered and after it exited the domain were measured in the morning and afternoon. Previous studies have shown that this method works well over flat terrain (e.g., Denmead et al. 1996; Levy et al. 1999). The applicability of the budget method for complex terrain has previously not been tested. Using a set of mesoscale model simulations for the Colorado Rockies, we found that the estimated surface CO_2 flux would converge to the true value with sufficient vertical CO_2 profile measurements at various locations upstream and downstream of the study domain. Using vertical CO_2 profiles measured by the C-130 aircraft upstream in the early morning and downstream in the afternoon, we found (not shown) that within the uncertainty of the budget method,

the estimated regional CO_2 flux is comparable with the CO_2 flux measured at the top of the CU tower for two of three fair weather days, one from each 2-week aircraft campaign. The airborne budget calculations seem to capture the seasonal variation of the regional CO_2 flux with strong CO_2 uptake toward the midsummer, which is in general agreement with the CU tower measurements. The one exception was on 20 May, when the budget and flux tower estimates of CO_2 uptake diverged. On this day, the CU CO_2 flux was roughly twice the regional CO_2 flux estimated using the morning and afternoon aircraft-observed CO_2 profiles at ~0845 and ~1300 LST. We hypothesize that the difference in the CO_2 flux is a consequence of large spatial variability in meteorological and ecological conditions across the region of the budget calculation. Comparison between the CU tower flux and the aircraft observations demonstrates the value of both long-term temporal ground observations and episodic spatial aircraft observations in estimating

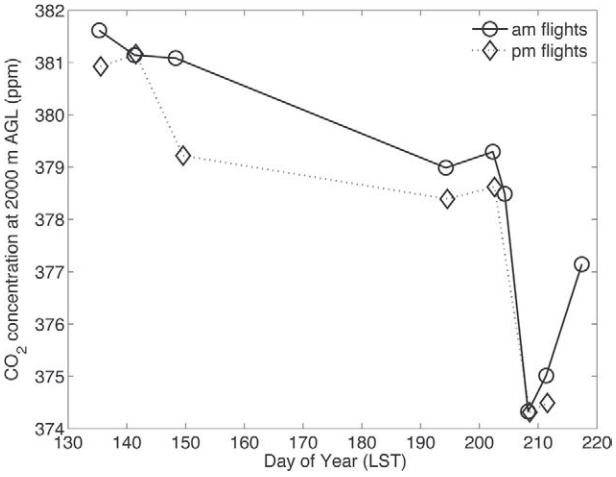

Fig. 11. The mean CO_2 concentration at 2000 m AGL as a function of the day of the year. It demonstrates the seasonal decrease of the CO_2 concentration from the spring to the early fall for the morning and afternoon flights and the regional diurnal variation of CO_2 concentration at 2000 m AGL.

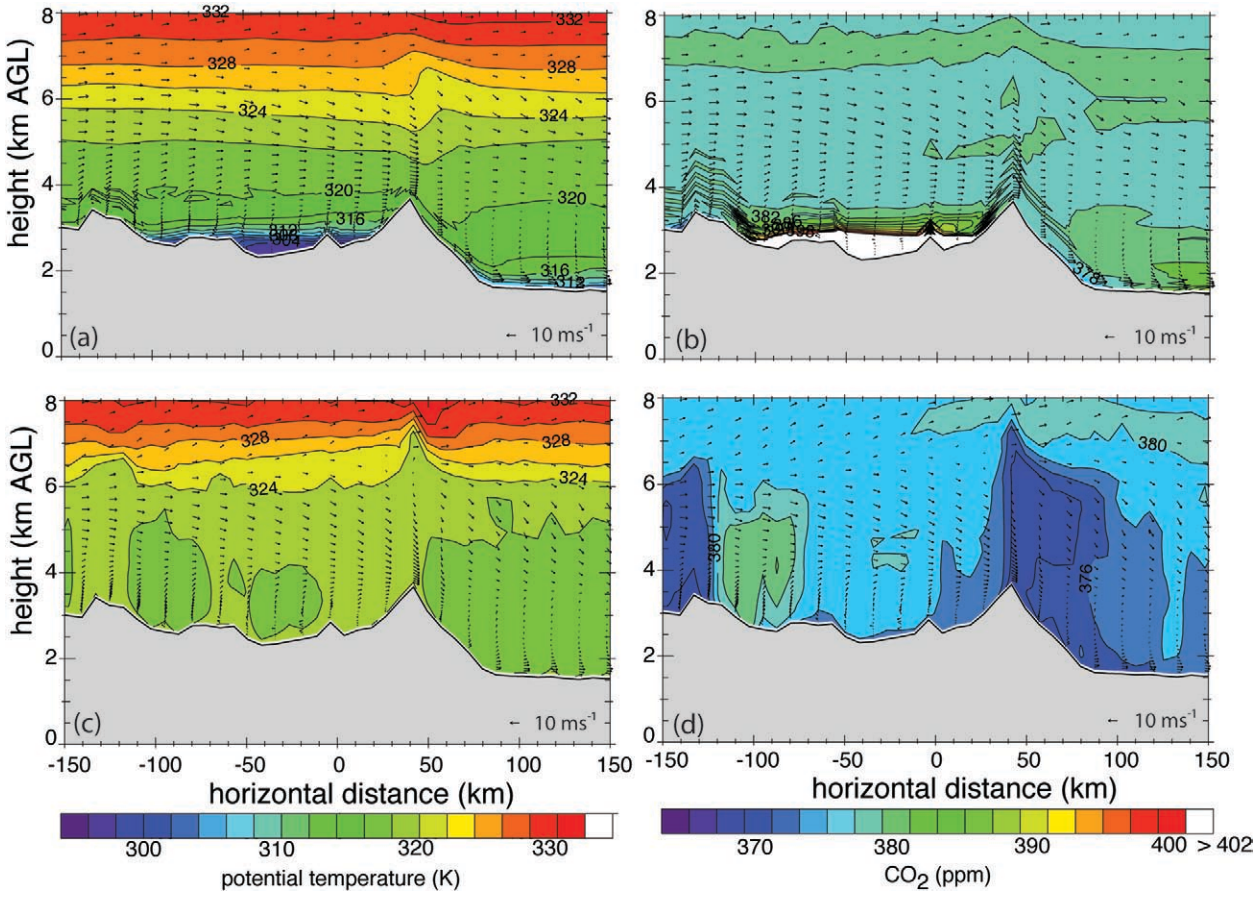

Fig. 12. The longitudinal cross sections (positive distance = east) of (a),(c) the modeled potential temperature and (b),(d) CO_2 concentration with wind vectors at (top) 0500 and (bottom) 1200 LST 12 Jul 2004. Blue shading indicates low potential temperature and CO_2 concentration. At 0500 LST, the modeled photosynthesis had started for a while as the sun rose at ~0430 LST, leading to the low CO_2 concentration on the east slope of the mountain. In contrast, the air surrounded by mountains (between −100 and 50 km) was still characterized as cold and CO_2-rich, reflecting the nighttime accumulation.

regional NEE. Aircraft measurements can be used to understand the spatial variation of the CO_2 fluxes and its relationship with surface features. Applying that knowledge to the long-term observations would effectively extend the long-term tower observations to a more realistic regional CO_2 budget estimate.

Modeled net ecosystem exchange. To help explain the mechanisms for the temporal variation of CO_2 fluxes measured by the CU tower, we performed a model–data synthesis using the Simplified Photosynthesis-EvapoTranspiration (SIPNET) ecosystem model and the measured CO_2 flux (Braswell et al. 2005; Sacks et al. 2006, 2007). We optimized the parameters of the SIPNET model to yield the best possible fit with the flux tower observations as described by Braswell et al. (2005). This optimization adapted the model to the specific conditions of the Niwot Ridge site, allowing a more accurate diagnosis of the mechanisms underlying the observed CO_2 fluxes. Through this model–data synthesis, we were able to partition the observed NEE flux into photosynthesis (gross primary productivity) and ecosystem respiration (Sacks et al. 2007). In addition, using a model selection criterion, we tested hypothesized mechanisms for the ecosystem's influence on CO_2 fluxes at Niwot Ridge. These experiments lent support to the hypotheses that 1) photosynthesis and possibly foliar respiration are down-regulated when the soil is frozen and 2) metabolic processes of soil microbes vary between summer and winter, beyond what can be explained simply by a temperature dependence of respiration, possibly because of the existence of distinct microbial communities at these two seasons (Sacks et al. 2006).

Finally, this model–data synthesis also provided information regarding how well the model parameters were constrained by the CO_2 flux observations. Some parameters could not be estimated well because of trade-offs with other parameters. For example, there were trade-offs between the initial stock of leaf carbon, the maximum photosynthetic rate, and the half-saturation point of the light–photosynthesis relationship. Thus, a robust model–data synthesis requires accurate field measurements of at least one of these parameters. Parameters governing long-term carbon dynamics, such as the turnover rate of leaf and stem carbon, were also poorly constrained by the subdecadal record of CO_2 fluxes.

Regional ecosystem flux of carbon from western Colorado. Daily CENTURY (DAYCENT; see www.nrel.colostate.edu/projects/century/) calculations were made for each 10 km × 10 km grid cell for the major land cover–soil association (Fig. 13). Subgrid simulations of these major land cover–soil associations within the 10 km × 10 km grid cell were implemented using appropriate climate data for each subgrid land cover–soil association. The forest simulation incorporated management and disturbance in a coarse fashion by relating stand ages derived from the Forest Inventory and Analysis (FIA) for each major forest type (land cover type) in each county of the study domain. The use of the stand ages allowed for an estimate of the timing of the last harvest or forest removal. These forest removal events were generated for each of the forest types per county. The fraction of a forest type in each county was used to apply area-weighted carbon sequestration values to forest types of appropriate age.

With the DAYCENT model, and using the land cover data as input, forest (Table 5) and shrubland

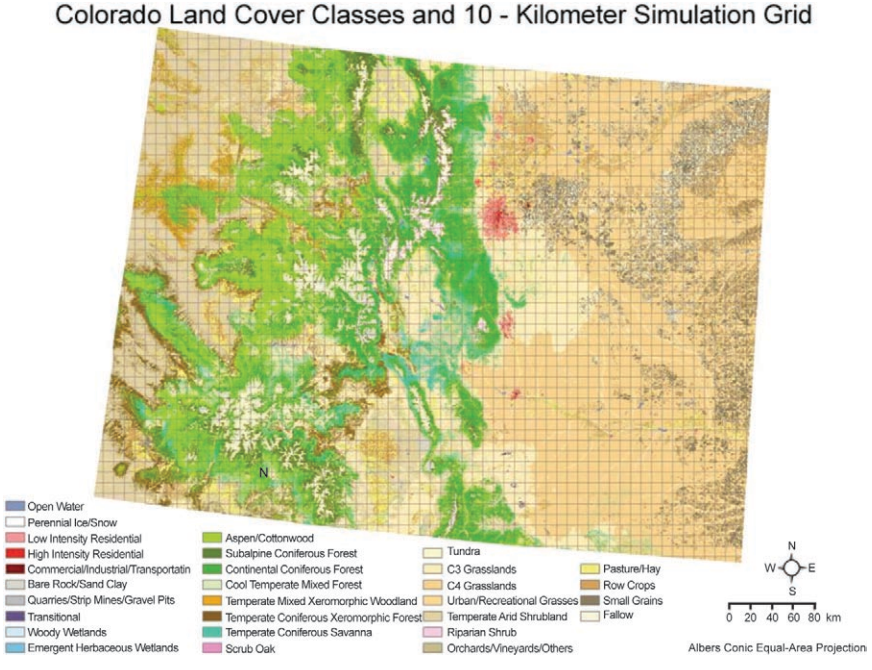

Fig. 13. Grid overlays on land cover used for the DAYCENT analyses.

were simulated to have modest C uptake. The forested areas had a carbon uptake of 12.6 Tg C per year, with the majority of this being sequestered in the mountainous forest. This carbon uptake for Colorado forest lands would account for approximately 5%–10% of the U.S. estimated annual forest sequestration rates, which range from 149 to 300 Tg C per year (Pacala et al. 2001; Woodbury et al. 2007). In shrubland ecosystems, carbon increases were low, likely due to drier weather conditions during the past decade and with continued grazing removals. The CO_2 sequestration of these ecosystems was estimated to be approximately 1.1 Tg C per year, with about 70% associated with aspen/cottonwood woodlands. The grasslands overall responded as a source of CO_2 to the atmosphere with an emission of approximately 1.2 Tg C per year, although the tundra grasslands tended to accumulate CO_2.

Table 5. Forest C sequestered (Tg C Eq yr^{-1}) as calculated by DAYCENT.

Subalpine coniferous	2.4
Montane coniferous	10.2
Mixed forests	0.5
Dry mixed woodlands	0.3
Dry coniferous woodlands	−1.6
Open/foothills coniferous forest	0.8
Total	12.6

SUMMARY AND FUTURE RESEARCH NEEDS OVER COMPLEX TERRAIN. We conducted a multiscale and multidisciplinary field campaign that was specially designed to focus on CO_2 transport in the atmospheric boundary layer over mountain forests. We strategically planned the ground-based field campaign to understand detailed CO_2 exchange and transport processes at multiple scales and an airborne field campaign to study regional CO_2 transport. A consistent picture of CO_2 transport has emerged: the distribution of CO_2 over mountain terrain is complicated but predictable. At night, the respired CO_2 was mainly transported downslope by the cold drainage flow following the carbonshed. The cold CO_2-rich air followed the carbonshed in intermittent bursts at the beginning of most nights and became steady toward the morning. The depth of the CO_2-rich flow in the carbonshed varied depending on the strength of the drainage flow and topography and was as high as 20 m at our site. By analyzing the oxygen isotope composition of near-surface soil moisture as a function of altitude and the oxygen isotope composition of the soil-respired CO_2, we found that the oxygen isotope values, $\delta^{18}O$, of the soil-respired CO_2 and of the top 10-cm soil moisture are correlated with each other, and the $\delta^{18}O$ value of the soil-respired CO_2 is a function of altitude because of higher precipitation at higher elevations and higher evaporation at lower elevations. The elevation-dependent patterns in soil respiration could be used as a valuable tool in future studies of nighttime CO_2 advection associated with atmospheric drainage flow at the site.

During day, we found that the CO_2-rich air was transported upslope as thermally driven slope flows switch from downslope to upslope under calm synoptic conditions, which contributes to the morning disappearance of the cold CO_2-rich air pool accumulated at night. The CO_2 transport by the morning circulation was documented by the observed mixing line of CO_2 concentration versus stable carbon isotope $\delta^{13}C$ of CO_2 based on the air samples collected at both the CME04 site and from the aircraft. The surface air of high CO_2 concentration and low $\delta^{13}C$ value was mixed up with the upper air of low CO_2 concentration and high $\delta^{13}C$ value. The role of the morning circulation was also supported by the large spatial variation of the CO_2 concentration over the rugged topographic relief as the CO_2-rich surface air was transported up by the morning upslope flow and the CO_2-poor upper air was transported down by the compensating descending air. This upslope flow was also shown to potentially contribute to the upward movement of biogenic/anthropogenic CO_2 from the Denver metropolitan corridor and the eastern plains during morning hours.

During our routine aircraft vertical profiling on the upwind boundary of the region, we found that the nighttime CO_2 pool in Colorado's intermountain valleys could persist until midmorning, whereas the nighttime CO_2 profile disappeared hours earlier elsewhere despite some CO_2 loss from valleys by mountain circulations over sunny slopes. We speculate that the delay of the convective mixing is due to the increased stability induced by sinking motions in the valley center that compensate for the air removed from the valley bottom by the upslope mountain flow, which was also confirmed by simulations with the RAMS numerical model.

Using the change in CO_2 concentration in an air mass moving with the mean flow, we derived the

regional CO_2 fluxes from three days of flights from the spring to the fall. We found that the regional CO_2 fluxes in general followed the seasonal variation of the CO_2 flux observed at the CU AmeriFlux tower site. By using a model–data synthesis approach with the SIPNET ecosystem model, we were able to investigate the primary controls over NEE at the Niwot Ridge AmeriFlux mountain site. We found that metabolic soil microbial processes were different in summer and winter. In addition, photosynthesis (and possibly foliar respiration) was downregulated when the soil was frozen in this evergreen forest. Simulations with the DAYCENT ecosystem model indicated that the ecosystem in western Colorado could have a carbon uptake of 12.6 Tg C per year, with the majority of the C uptake being sequestered in the mountain forest.

Our analyses of the ground and airborne field campaigns and our modeling efforts are still in progress, but they have already demonstrated that multiscale and multidisciplinary observations guided by ecological and atmospheric principles and integrated with assimilation models can be used to characterize regional ecosystem–atmosphere exchange over mountains and to quantify regional NEE and its control parameters by taking advantage of mountain dynamic flow. The role of the mountain circulation in CO_2 transport discussed in the study can be played over seemingly flat terrain by mesoscale flows generated by various physical processes. Therefore, the three-dimensional observation strategy considered here may have application over seemingly flat terrain.

ACKNOWLEDGMENTS. We would like to thank David Fitzjarrald and two anonymous reviewers for their constructive suggestions and comments. The study was supported by NSF Grant EAR-0321918. We would like to thank the staff members of ISFF and RAF at NCAR/EOL for their hard work and support to the field campaigns of CME04 and ACME04. Support for the NCAR/EOL facilities was provided by the National Science Foundation's Deployment Pool. Ecosystem modeling was supported also by NASA Grant NNG04GH63G to NREL at Colorado State University.

REFERENCES

Ahmadov, R., C. Gerbig, R. Kretschmer, S. Koerner, B. Neininger, A. J. Dolman, and C. Sarrat, 2007: Mesoscale covariance of transport and CO_2 fluxes: Evidence from observations and simulations using the WRF–VPRM coupled atmosphere–biosphere model. *J. Geophys. Res.,* **112,** D22107, doi:10.1029/2007JD008552.

Aubinet, M., B. Heinesch, and M. Yernaux, 2003: Horizontal and vertical CO_2 advection in a sloping forest. *Bound.-Layer Meteor.,* **108,** 397–417.

Baldocchi, D. D., 2003: Assessing the eddy covariance technique for evaluating carbon dioxide exchange rates of ecosystems: Past, present, and future. *Global Change Biol.,* **9,** 479–492.

Bowen, G. J., and B. Wilkinson, 2002: Spatial distribution of $\delta^{18}O$ in meteoric precipitation. *Geology,* **30,** 315–318.

Bowling, D. R., D. E. Pataki, and J. T. Randerson, 2008: Carbon isotopes in terrestrial ecosystem pools and CO_2 fluxes. *New Phytol.,* **178,** 24–40.

Braswell, B. H., W. J. Sacks, E. Linder, and D. S. Schimel, 2005: Estimating diurnal to annual ecosystem parameters by synthesis of a carbon flux model with eddy covariance covariance net ecosystem exchange observations. *Global Change Biol.,* **11,** 335–355.

Burns, S. P., and Coauthors, 2006: Measurements of the diurnal cycle of temperature, humidity, wind, and carbon dioxide in a subalpine forest during the Carbon in the Mountains Experiment (CME04). Preprints, *27th Conf. on Agricultural and Forest Meteorology*, San Diego, CA, Amer. Meteor. Soc., JP4.7 [Available online at http://ams.confex.com/ams/BLTAgFBioA/techprogram/paper_110188.htm.]

——, and ——, 2009: An evaluation of calibration techniques for in situ carbon dioxide measurements using a programmable portable trace gas measuring system. *J. Atmos. Oceanic Technol.,* **26,** 291–316.

Chapin, F. S., and Coauthors, 2006: Reconciling carbon-cycle concepts, terminology, and methods. *Ecosystems,* **9,** 1041–1050.

Ciais, P., P. P. Tans, M. Trolier, J. W. C. White, and R. J. Francey, 1995: A large northern hemisphere terrestrial CO_2 sink indicated by the $^{13}C/^{12}C$ ratio of atmospheric CO_2. *Science,* **269,** 1098–1102.

Clark, D. A., S. Brown, D. W. Kicklighter, J. Q. Chambers, J. R. Thomlinson, and J. Ni, 2001: Measuring net primary production in forests: Concepts and field methods. *Ecol. Appl.*, **11,** 356–370.

Craig, H., 1961: Isotopic variations in meteoric waters. *Science,* **133,** 1702–1703.

Daube, B. C., Jr., K. A. Boering, A. E. Andrews, and S. C. Wofsy, 2002: A high-precision fast-response airborne CO_2 analyzer for in situ sampling from the surface to the middle stratosphere. *J. Atmos. Oceanic Technol.,* **19,** 1532–1543.

Denmead, O. T., M. R. Raupach, F. X. Dunin, H. A. Cleugh, and R. Leuning, 1996: Boundary layer budgets for regional estimates of scalar fluxes. *Global Change Biol.,* **2,** 255–264.

Dolman, A. F., and Coauthors, 2006: The CarboEurope Regional Experiment Strategy. *Bull. Amer. Meteor. Soc.,* **87,** 1367–1379.

Doran, J. C., and T. W. Horst, 1981: Velocity and temperature oscillations in drainage winds. *J. Appl. Meteor.,* **20,** 361–364.

Feigenwinter, C., C. Bernhofer, R. Vogt, 2004: The influence of advection on the short-term CO_2 budget in and above a forest canopy. *Bound.-Layer Meteor.,* **113,** 201–224.

Fry, B., 2006: *Stable Isotope Ecology.* Springer, 308 pp.

Fung, I., and Coauthors, 1997: Carbon 13 exchanges between the atmosphere and biosphere. *Global Biogeochem. Cycles,* **11,** 507–533.

Gerbig, C., S. Schmitgen, D. Kley, and A. Volz-Thomas, 1999: An improved fast-response vacuum-UV reasonance fluorescence CO instrument. *J. Geophys. Res.,* **104,** 1699–1704.

Gough, C. M., C. S. Vogel, H. P. Schmid, H.-B. Su, and P. S. Curtis, 2008: Multi-year convergence of biometric and meteorological estimates of forest carbon storage. *Agric. For. Meteor.,* **148,** 158–170.

Graven, H. D., B. B. Stephens, T. P. Guilderson, T. L. Campos, D. S. Schimel, J. E. Campbell, and R. F. Keeling, 2009: Vertical profiles of biospheric and fossil fuel-derived CO_2 and fossil fuel CO_2: CO ratios from airborne measurements of $\Delta^{14}C$, CO_2 and CO above Colorado, USA. *Tellus,* **61B,** 536–546, doi:10.1111/j.1600-0889.2009.00421.x.

Lai, C.-T., A. Schauer, C. Owensby, J. M. Ham, B. R. Helliker, P. P. Tans, and J. R. Ehleringer, 2006: Regional CO_2 fluxes inferred from mixing ratio measurements: Estimates from flask air samples in central Kansas, USA. *Tellus,* **58B,** 523–536.

Lauvaux, T., and Coauthors, 2008: Mesoscale inversion: First results from the CERES campaign with synthetic data. *Atmos. Chem. Phys.,* **8,** 3459–3471.

Levy, P. E., A. Grelle, A. Lindroth, M. Molder, P. G. Jarvis, B. K. Kruijt, and J. B. Moncrieff, 1999: Regional-scale CO_2 fluxes over central Sweden by a boundary layer budget method. *Agric. For. Meteor.,* **98–99,** 169–180.

Lin, J. C., C. Gerbig, S. C. Wofsy, A. E. Andrews, B. C. Daube, K. J. Davis, and C. A. Grainger, 2003: A near-field tool for simulating the upstream influence of atmospheric observations: The Stochastic Time-Inverted Lagrangian Transport (STILT) model. *J. Geophys. Res.,* **108,** 4493, doi:10.1029/2002JD003161.

Miller, J. B., D. Yakir, J. W. C. White, and P. P. Tans, 1999: Measurement of $^{18}O/^{16}O$ in the soil–atmosphere CO_2 flux. *Global Biogeochem. Cycles,* **13,** 761–771.

Monson, R. K., A. A. Turnipseed, J. P. Sparks, P. C. Harley, L. E. Scott-Denton, K. Sparks, and T. E. Huxman, 2002: Carbon sequestration in a high-elevation, subalpine forest. *Global Change Biol.,* **8,** 459–478.

——, and Coauthors, 2005: Climatic influences on net ecosystem CO_2 exchange during the transition from wintertime carbon source to springtime carbon sink in a high-elevation, subalpine forest. *Oecologia,* **146,** 130–147.

——, S. P. Burns, M. W. Williams, A. C. Delany, M. Weintraub, and D. A. Lipson, 2006a: The contribution of beneath-snow soil respiration to total ecosystem respiration in a high-elevation, subalpine forest. *Global Biogeochem. Cycles,* **20,** GB3030, doi:10.1029/2005GB002684.

——, D. L. Lipson, S. P. Burns, A. A. Turnipseed, A. C. Delany, M. W. Williams, and S. K. Schmidt, 2006b: Winter forest soil respiration controlled by climate and microbial community composition. *Nature,* **439,** 711–714, doi:10.1038/nature04555.

Moore, D. J. P., J. Hu, W. J. Sacks, D. S. Schimel, and R. K. Monson, 2008: Estimating transpiration and the sensitivity of carbon uptake to water availability in a subalpine forest using a simple ecosystem process model informed by measured net CO_2 and H_2O fluxes. *Agric. For. Meteor.,* **148,** 1467–1477.

Oncley, S. P., K. Schwenz, S. P. Burns, J. Sun, and R. K. Monson, 2009: A cable-borne tram for atmospheric measurements along transects. *J. Atmos. Oceanic Technol.,* **26,** 462–473.

Pacala, S. W., and Coauthors, 2001: Consistent land- and atmosphere-based U.S. carbon sink estimates. *Science,* **292,** 2316–2320.

Pielke, R. A., and Coauthors, 1992: A comprehensive meteorological modeling system—RAMS. *Meteor. Atmos. Phys.,* **49,** 69–91.

Pypker, T. G., M. H. Unsworth, A. C. Mix, W. Rugh, T. Ocheltree, K. Alstad, and B. J. Bond, 2007a: Using nocturnal cold air drainage flow to monitor ecosystem processes in complex terrain. *Ecol. Appl.,* **17,** 702–714.

——, ——, B. Lamb, E. Allwine, S. Edburg, E. Sulzman, A. C. Mix, and B. J. Bond, 2007b: Cold air drainage in a forested valley: Investigating the feasibility of monitoring ecosystem metabolism. *Agric. For. Meteor.,* **145,** 149–166.

Ryan, M. G., and B. E. Law, 2005: Interpreting, measuring, and modeling soil respiration. *Biogeochemistry,* **73,** 3–27.

Sacks, W. J., D. S. Schimel, R. K. Monson, and B. H. Braswell, 2006: Model-data synthesis of diurnal and seasonal CO_2 fluxes at Niwot Ridge, Colorado. *Global Change Biol.,* **12,** 240–259.

——, ——, and ——, 2007: Coupling between carbon cycling and climate in a high-elevation, subalpine forest: A model–data fusion analysis. *Oecologia,* **151,** 54–68.

Schaeffer, S. M., D. E. Anderson, S. P. Burns, R. K. Monson, J. Sun, and D. R. Bowling, 2008: Canopy structure and atmospheric flows in relation to the $\delta^{13}C$ of respired CO_2 in a subalpine coniferous forest. *Agric. For. Meteor.,* **148,** 592–605.

Schauer, A. J., C.-T. Lai, D. R. Bowling, and J. R. Ehleringer, 2003: An automated sampler for collection of atmospheric trace gas samples for stable isotope analyses. *Agric. For. Meteor.,* **118,** 113–124.

——, M. J. Lott, C. S. Cook, and J. R. Ehleringer, 2005: An automated system for stable isotope and concentration analyses of CO_2 from small atmospheric samples. *Rapid Commun. Mass Spectrom.,* **19,** 359–362.

Schimel, D., T. G. F. Kittel, S. Running, R. Monson, A. Turnipseed, and D. Anderson, 2002: Carbon sequestration studied in western U.S. mountains. *Eos, Trans. Amer. Geophys. Union,* **83,** 445–449.

Scholze, M., J. O. Kaplan, W. Knorr, and M. Heimann, 2003: Climate and interannual variability of the atmosphere–biosphere $^{13}CO_2$ flux. *Geophys. Res. Lett.,* **30,** 1097, doi:10.1029/2002GL015631.

Staebler, R. M., and D. R. Fitzjarrald, 2004: Observing subcanopy CO_2 advection. *Agric. For. Meteor.,* **122,** 139–156.

Stephens, B., A. Watt, and G. Maclean, 2006: An autonomous inexpensive robust CO_2 analyzer (AIRCOA). *Proc. 13th WMO/IAEA Meeting of Experts on Carbon Dioxide Concentration and Related Tracers Measurement Techniques,* WMO Tech. Doc. 1359, GAW Rep. 168, Boulder, CO, Global Atmosphere Watch Programme, 95–99.

Sun, J., and Coauthors, 2007: CO_2 transport over complex terrain. *Agric. For. Meteor.,* **145,** 1–21.

Turnipseed, A. A., D. E. Anderson, P. D. Blanken, W. M. Baugh, and R. K. Monson, 2003: Airflows and turbulent flux measurements in mountainous terrain. Part I: Canopy and local effects. *Agric. For. Meteor.,* **119,** 1–21.

Vendramini, P. F., and L. Sternberg, 2007: A faster plant stem-water extraction method. *Rapid Commun. Mass Spectrom.,* **21,** 164–168.

Whiteman, C. D., 2000: *Mountain Meteorology: Fundamentals and Applications*. Oxford University Press, 355 pp.

Woodbury, P.B., J. E. Smith, and L. S. Heath, 2007: Carbon sequestration in the U.S. forest sector from 1990 to 2010. *For. Ecol. Manage.,* **241,** 14–27.

Yi, C., R. K. Monson, D. E. Anderson, Z. Zhai, B. Lamb, A. A. Turnipseed, and S. P. Burns, 2005: Modeling and measuring the nighttime drainage flow in a high-elevation, subalpine forest ecosystem with complex terrain. *J. Geophys. Res.,* **110,** D22303, doi:10.1029/2005JD006282.

——, D. E. Anderson, A. A. Turnipseed, S. P. Burns, J. P. Sparks, D. I. Stannard, and R. K. Monson, 2008: The contribution of advective fluxes to net ecosystem CO_2 exchange in a high-elevation, subalpine forest. *Ecol. Appl.,* **18,** 1379–1390.